

INVESTIGATION OF UNDERWATER ACOUSTIC MULTI-PATH DOPPLER AND DELAY SPREADING IN A SHALLOW MARINE ENVIRONMENT

Michael Caley and Alec Duncan

Curtin University, Department of Imaging and Applied Physics, Centre for Marine Science and Technology, Perth, Australia
michaelcaley@westnet.com.au

Doppler frequency spreading and arrival delay spreading of underwater acoustic communication signals under the influence of surface waves and transmitter-receiver motion were investigated in a channel probing experiment conducted primarily with binary pseudo-noise (PN) sequences ranging from 21ms to 1.4s duration. Testing was conducted in a 13.5m deep environment at transmission distances ranging from 44m to 1007m. The channel Doppler response was investigated both by time-domain Doppler search of the transmit-receive correlation for successive repeats of a 1.4s probe sequence, and by Fourier analysis of the channel impulse response history from a repeated 21ms probe sequence (i.e. Spreading Function). The bounds of Doppler shift imparted by relative transmitter/receiver motion and surface wave motion to idealised sound-ray transmission paths has been compared with experimental Doppler indicated by the Spreading Function. The coherence of the experimental channel response was also examined for different propagation ranges and at different delayed arrivals of the experimental signals.

INTRODUCTION

The choice for the wireless transmission of data underwater is between electromagnetic waves (e.g. light or radio) or sound waves. Light and radio waves are valuable for high-rate data transmission through water over short ranges of the order of a few metres. When transmission is required over longer distances through water, sound waves are the only viable wireless option.

Underwater acoustic data transmission is not without significant constraints intrinsic to the marine environment. The underwater acoustic environment is highly reverberant, resulting in multiple reflected copies of any transmitted signal arriving at the receiver at delayed intervals (delay spreading), and with the relative delays generally changing with time. The frequency of transmitted signals is also significantly distorted by transient Doppler effects generated by elongation and contraction of surface reflected transmission paths (Doppler frequency spreading), or Doppler frequency shifts from movement of either (or both) the transmitter and receiver. Transient delay spreading and Doppler spreading of the received signal present significant challenges to the decoding of incoming data symbols by a communications receiver, with the problem becoming more difficult as the rate of data transmission increases.

In 2011 the Department of Electrical and Computer Engineering and the Centre for Marine Science and Technology (CMST) at Curtin University commenced a project to develop high-rate underwater acoustic communications to support developing ocean-based industries in Australia [1]. The authors' role is to develop an underwater acoustic communication channel simulator to support this project. The purpose of the simulator is to simulate the way that the real ocean produces transient distortion of acoustic communication signals between

a transmitter and a receiver, including interference effects from highly variable natural and anthropogenic noise. The simulator provides a configurable analogue of the real ocean that can be used to improve understanding of the influence of the marine acoustic environment on communications signals, and assists the development of underwater communication modulation and demodulation algorithms and hardware.

Transient phenomena that are key to the development of an acoustic channel simulator for high-rate data communications are the transient delay and Doppler frequency spreading of the received signal imparted by the moving sea-surface, shown schematically in Fig. 1, and the transient Doppler imparted by moving transmitter and/or receiver platforms [2,3].

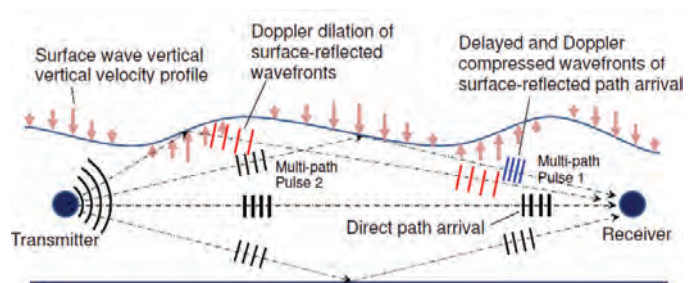


Figure 1. Conceptual signal Doppler shift and path delay

Experimental channel probing was conducted primarily with binary pseudo-noise (PN) sequences ranging from 21ms to 1.4s duration. The signal was created by phase-modulating a continuous 12kHz sinusoid with the binary sequence. This method is described in communication literature as Direct Sequence Spread Spectrum (DSSS) signalling.

In this investigation the channel Doppler response to probe

signals was investigated both by a time-domain resampling Doppler search method on successive transmit-receive (txrx) PN sequence blocks, and also by Fourier analysis of the channel response with respect to time, to generate the frequency-domain Doppler Spreading Function.

It is customary to present the channel Doppler axis of the Spreading Function $S(\tau, f)$ in the units of Hz. $S(\tau, f)$ was calculated in Eq. (1) by discrete Fourier analysis of the channel response $h(\tau, t)$.

$$S(\tau, f) = \sum_{n=-N-1}^{n=0} h(m, n) \exp\left(-\frac{i2\pi np}{N}\right) \quad (1)$$

$S(\tau, f)$ was calculated from $N = 1400$ impulse responses $h(\tau, t)$ spaced in the time (t) dimension at intervals $T = 21\text{ms}$, with time $t = nT$. The impulse response in the delay dimension (τ) was calculated from sampling at frequency $f_s = 96\text{kHz}$, with response delay $\tau = m/f_s$ and Doppler frequencies $f = p/NT$ where $p \in [-N/2+1, \dots, N/2]$.

When the complex channel response $h(\tau, t)$ is determined by cross-correlation of a modulated transmit and receive signal, the rate at which the phase of $h(\tau, t)$ changes with respect to time (t) is scaled by the probe signal carrier frequency (f_0). Accordingly the Doppler shift spectrum at each delay (τ) calculated by DFT of $h(\tau, t)$ is also scaled by the probe signal carrier frequency.

For a physical layer modeller it is helpful to note that the Doppler shift derived by (1) is responsive to $h(\tau, t)$ phase changes originating not only from Doppler phase compression/dilation, but also from what will be described as ‘apparent’ Doppler due to phase changes associated with transient phase interference of clustered multipath arrivals, and transient angular scattering of propagation paths by a moving sea surface [4].

The channel Doppler response may be expressed either as an equivalent velocity shift δv or as an equivalent signal-dependent frequency shift δf as linked by Eq. (2), where positive δv represents an equivalent velocity shift that contracts the propagation path length and c is the speed of sound in water.

$$\delta f(f_0) = \delta v/c \quad (2)$$

In this paper the measured channel Doppler response has generally been reported as a frequency shift (Hz), but in the case of Spreading Function plots a secondary axis with Doppler velocity shift was added to enable comparison with Doppler velocity shift estimates from geometrical considerations.

CHANNEL PROBING TESTS

A shallow (13.5m) channel probing experiment was conducted in April 2012 over distances ranging from 44m to 1007m. The transmitter and receiver arrangements are illustrated in Figs. 2 and 3, respectively. The transmitter was inverted (relative to conventional vertical downwards primary axis alignment) to maximise the signal strength for surface reflected transmission paths.

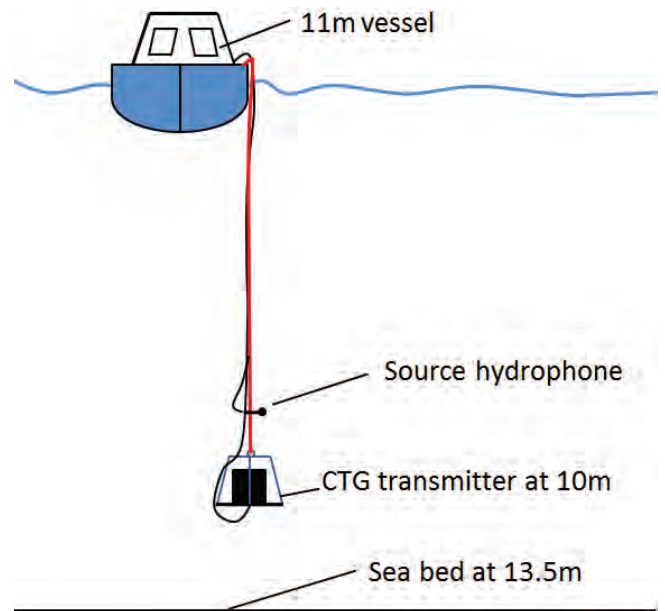


Figure 2. Transmitter configuration

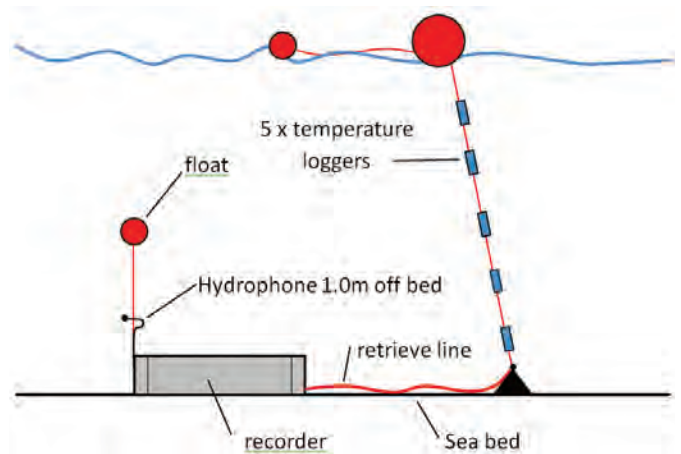


Figure 3. Receiver configuration

Experimental arrangement and instrumentation

Transmitted and received signals were sampled with 24 bit resolution at 96kHz. Directional surface wave data was obtained from a Directional Wave Rider Buoy (DWRB) located approximately 1.5km NE of the receiver. The sound-speed profile at each site was sampled with a Conductivity Temperature Depth (CTD) probe. The vessel was fitted with pitch, heave and roll data acquisition sampling at 100Hz. Five temperature loggers sampling at 60 second intervals were suspended from the surface float line. Grab samples were collected of the sandy bottom material.

Probe signals

Probe signals for simultaneous Doppler shift and delay detection consisted of a 12kHz continuous wave (CW) carrier modulated at a 3kHz chipping rate by binary phase pseudorandom (PN) sequences. The longer temporal effects

associated with wave and swell were explored by continuing the sequence repetitions over an interval greater than the swell period. A repeated pattern was transmitted consisting of 60s of 1.4s PN sequence (n-bits = 4095), 30s of 170ms PN sequence (n-bits = 511) and 30s of 21ms PN sequence (n-bits = 63). This was followed by 30 repeats of a 16ms 8kHz-16kHz linear frequency sweep at 1s intervals. The sweeps were utilised to provide an unambiguous check on the channel delay spread and structure.

The bandwidths of trial signals were guided by the ± 3 dB transmit sensitivity of the Chelsea Technologies CTG052 transmit transducer. Signals were written to a 24 bit wav file then replayed on a digital audio player with output amplification to the transmitter.

Doppler and delay resolution – single block processing

The delay resolution δ_t of multi-path arrivals for a PN probe signal is determined by the sequence chipping interval t_{chip} as per Eq. (3). For a linear frequency sweep, δ_t is the inverse of the maximum sweep frequency.

$$\delta_t = \frac{t_{chip}}{2} \tag{3}$$

The Doppler velocity shift resolution δ_v for a PN sequence probe signal depends on the sequence repeat interval T and the signal carrier frequency f_0 as per Eq. (4) where c is the speed of sound. For a linear frequency sweep, f_0 is replaced by the maximum sweep frequency.

$$\delta_v = \frac{c}{f_0 T} \tag{4}$$

The probe signal frequencies, repeat intervals, bandwidths and associated delay and Doppler resolutions are detailed in Table 1.

Table 1. Trial test signals

Signal type	f_0 (kHz)	Period T (s)	Chipping rate	δ_t (ms)	δ_v (m/s)
PN	12	1.4	3	0.16	0.094
PN	12	0.17	3	0.16	0.75
PN	12	0.021	3	0.16	6.1
Sweep	8-16	0.016	-	0.06	6.0

Doppler resolution – 21ms ensemble block processing

The Doppler velocity resolution of the Spreading Function from the 21ms probe impulse response history is also calculated by Eq. (4), but with T evaluated with the block ensemble duration of 30s. The resultant Doppler resolution is 0.0043m/s, or 0.033Hz, with Nyquist frequency of 23.8Hz.

Test sea conditions

The water column was well mixed during testing with the sound speed ranging almost linearly from 1537m/s at the surface to 1536m/s at the bottom. Wind conditions were light

to still, with low swell and sea conditions reported at 15 minute intervals from the nearby (1.5km distant) Cottesloe Directional Wave Rider Buoy (DWRB) as summarised in Table 2. The appearance of the sea surface during testing is illustrated in Fig. 4. It is notably free of surface bubbles.

Table 2. Wave height data for presented results

Wave type	Significant height H_s	Wave period T_m	Wave frequency
Swell	0.4m	13-14s	0.07Hz
Sea	0.25m	3s	0.33Hz



Figure 4. Experimental sea surface

IDEALISED CHANNEL DELAY STRUCTURE

The arrival delay structure for an idealised ocean waveguide with specular surface and bottom reflections and constant sound speed shown schematically in Fig. 5 is graphed in Fig. 6 to assist with the interpretation of the measured delay structure. ‘B’ stands for a bottom-bounce, and ‘S’ a surface-bounce. It may be noted that at increasing ranges the time separation between delays becomes less than the delay resolution of test signals listed in Table 1.

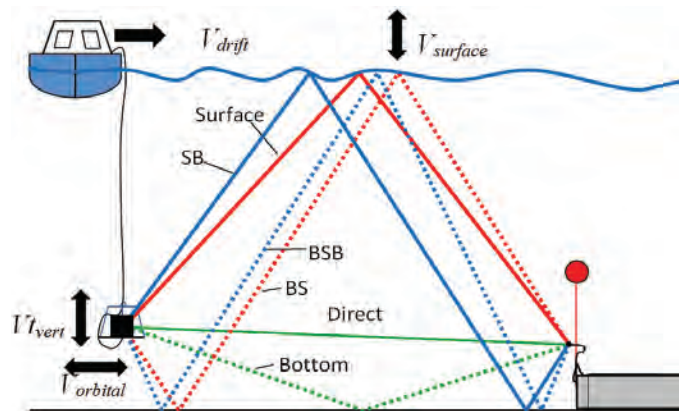


Figure 5. Low order reflected paths

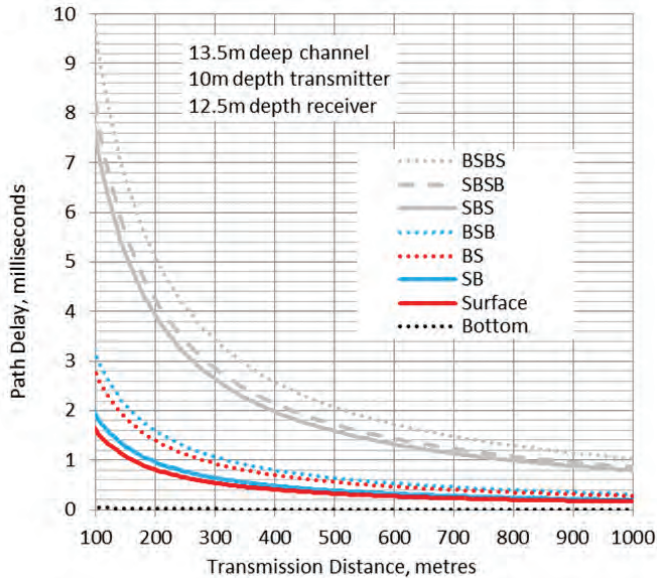


Figure 6. Idealised delay structure of reflected paths relative to the direct path

DOPPLER CONTRIBUTIONS FROM RELATIVE MOTION

The primary geometrical sources of relative motion that contribute to the experimental Doppler shift are sea-surface motion, wave orbital motion coupling to the suspended transmitter, and transmitter movement generated by vessel rolling and drift as illustrated in Fig. 5. These components were resolved into the idealised acoustic transmission paths, then combined to provide a Doppler velocity shift interpretation of the Doppler effect indicated by the experimental Spreading Function.

The slow-changing contributions (drift and swell orbital motion) have been treated as constant values, whereas the rapidly changing stochastic Doppler velocity contributions from sea-surface reflections and vertical transmitter oscillation have been quantified as 3σ estimates where σ is the standard deviation. Successive surface reflections and vertical transmitter oscillations have been treated as independent processes. Only the vertical motion of surface reflections has been considered. The more complex horizontal surface-wave velocity components are not considered.

Vessel drift closing speed

The average closing speed V_{drift} was calculated from GPS data for the vessel drift. This speed ranged from 0.11m/s to 0.19m/s for the data presented. This relative motion contributes almost the same Doppler shift to all transmission paths as per Eq. (5), where θ is the path launch angle from horizontal.

$$V_d = V_{drift} \cos\theta \quad (5)$$

Transmit-receive motion coupled to orbital wave motion

The cable tether of both the transmitter (tx) at 10m depth and the receiver (rx) hydrophone 1m off the bottom make both

susceptible to orbital wave motion, however the movement of the receiver hydrophone would be limited compared to that of the transmitter. At the depth of the transmitter the horizontal component of swell orbital motion is significant in the shallow test channel, with the contribution from wind-waves not extending below mid-depth. If it is conservatively assumed that the transmitter is completely compliant horizontally, the relative horizontal orbital motion $V_{orbital}$ is calculated at up to 0.17m/s for the Table 2 data. This relative motion contributes almost the same Doppler to all transmission paths as per Eq. (6).

$$V_o = V_{orbital} \cos\theta \quad (6)$$

Surface vertical velocity

The maximum vertical surface velocity $V_{surface}$ at the point of surface reflections was estimated based on the 3σ wave height for swell and sea by Eq. (7), providing estimates of 0.39m/s for the $H_s = 0.25$ m sea-waves, and 0.13m/s for the $H_s = 0.4$ m swell. The higher estimate obtained from the wind-waves was utilised as an upper bound estimate of $V_{surface}$. The vertical surface motion from a single surface reflection can be resolved in the direction of an idealised surface-reflected path as per Eq. (8).

$$V_{surface} = 3\pi H_s / 2T_m \quad (7)$$

$$V_s = 2V_{surface} \sin\theta \quad (8)$$

Vertical transmitter motion

The vertical velocity spectral density of the transmitter in Fig. 7 was calculated from the combined vessel pitch, heave and roll data by averaging 18 x 160s blocks of data with Hamming windowing. This data shows a peak at 0.07Hz that corresponds to the DWRB swell data, and peaks at frequencies similar to the DWRB data for wind-driven surface waves. These higher frequency peaks were likely influenced by the resonant pitch and roll frequencies of the vessel. The vertical root-mean-square (RMS) velocity from the data in the 0-2Hz range was 0.13m/s, providing a 3σ estimate of 0.39m/s for this component.

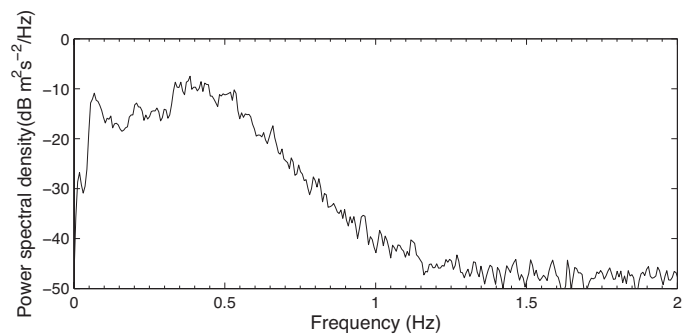


Figure 7. Transmitter vertical velocity power spectrum

The vertical transmitter velocity $V_{t_{vert}}$ can be resolved in the direction of all surface and/or bottom reflected transmission paths as per Eq. (9).

$$V_t = V_{t_{vert}} \sin\theta \quad (9)$$

Combination of geometrical Doppler velocity components resolved in path

An estimate of the 3σ total in-path Doppler shift for a path involving n_b surface bounces was calculated from components assuming independence of stochastic processes as per Eq. (10).

$$V_{total} = V_d + V_o + \sqrt{V_t^2 + n_b V_s^2} \quad (10)$$

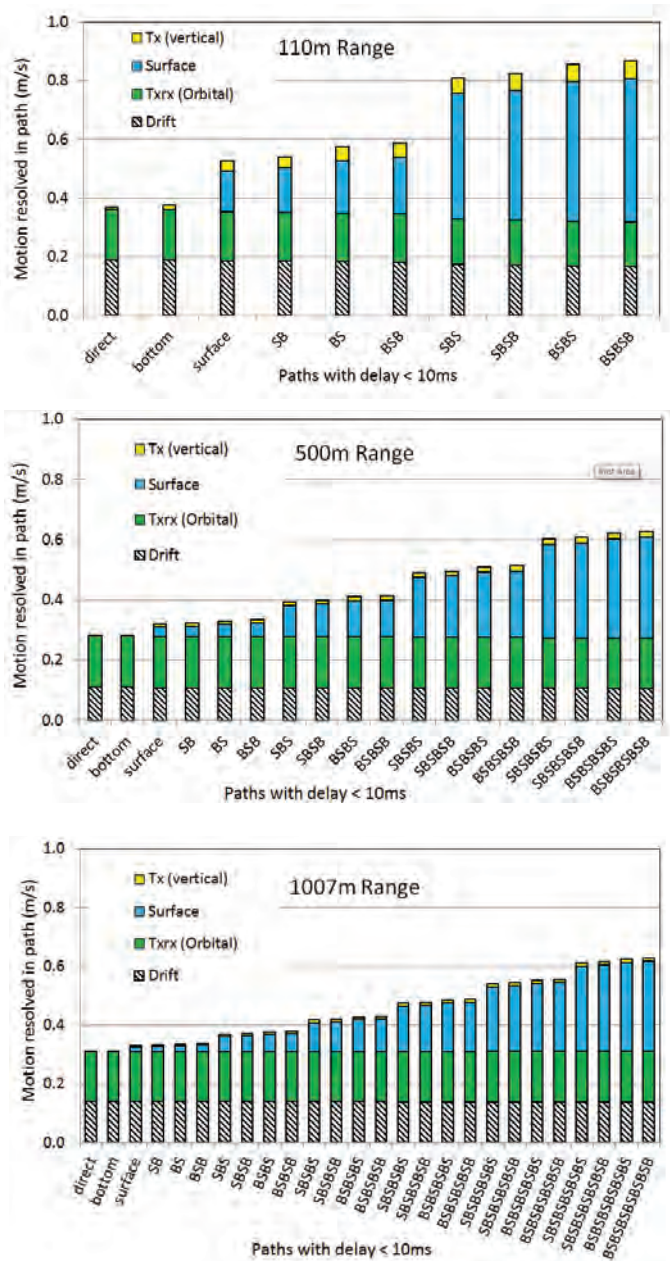


Figure 8. 3σ estimates of maximum geometrical Doppler velocity shifts resolved along idealised paths for path delays < 10ms

The geometrical Doppler components discussed in previous sections are compared in Fig. 8 for all idealised ray paths within 10ms delay relative to the direct path, for the example test distances of 110m, 500m, 1007m. The experimental txrx drift rate varied at each distance. Records of wave conditions from the nearby DWRB were comparable for all transmission ranges. This analysis indicates that the potential maximum in-path Doppler shift increases significantly with the number of surface bounces at short range, with the vertical surface Doppler delay per surface bounce diminishing with range.

It is noted that the test results relate to relatively low experimental surface wave heights as per Table 2. Sea and swell are commonly 4-5 times higher at the test site which would lead to all related Doppler velocity components increasing commensurately.

EXPERIMENTAL DELAY RESULTS

The transmit-receive correlation versus delay histories are presented for 110m, 500m and 1007m transmit ranges in Figs. 9-11. The correlation response for each time block was normalised by the product of the transmit and receive signal power. The plots are the absolute value of the correlation R , so do not reveal the phase changes occurring in R with time.

Successive block impulse responses were aligned on the first correlation maxima (with a 0.01ms numerical time step), without resampling to adjust for cyclical Doppler shift from txrx movement. Consequently the resultant channel response history will include distortion of the delay between the first maxima and subsequent arrivals due to this txrx relative movement. However the magnitude of this delay distortion is less than 0.01ms, less than a tenth of the delay resolution for the experimental probe signal. It is concluded that the ‘approximate’ delay history obtained in this manner is reliable.

The correlation results from 16ms frequency sweeps at 1s intervals (not shown) were used to check on the delay structure out to 60ms, confirming that the 10ms delay structure revealed by the 21ms probe sequence contains the significant arrivals for this channel.

Utilising the idealised delay structure in Fig. 6 for 110m range for reference, the first correlation maximum in Fig. 9 represents the combined direct and bottom-reflected paths, with the second group of arrivals extending between 1ms and 3ms corresponding to Surface, BS, SB and BSB reflected paths. The next group of arrivals for paths involving two surface reflections are apparent between 6ms and 10ms.

At 500m range (Fig. 10) the contracting of the delay spread is apparent with two additional bands of higher order surface reflections evident. The results at this range are notable as the first correlation maximum is suppressed relative to the second as a consequence of destructive phase interference between the Direct and Bottom paths. In this channel the Surface, SB, BS and BSB paths combine to provide a stronger arrival, but with interruption at intervals matching the swell period, presumably relating to destructive interference associated with differential path elongation/contraction.

At 1007m range the relative phases of the Direct, Surface and Bottom bounce again combine constructively to produce a strongest first correlation maximum.

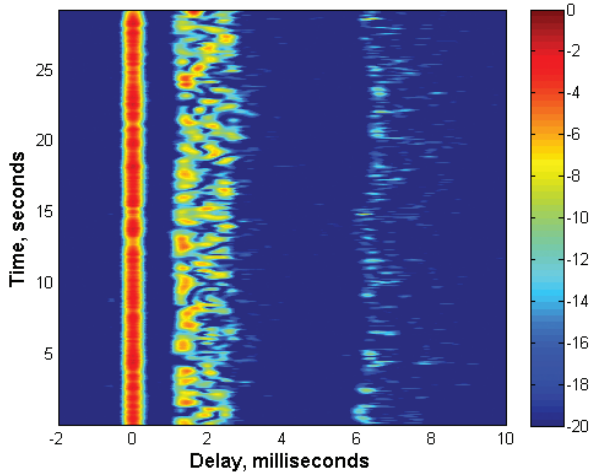


Figure 9. Normalised txrx correlation history (dB)–21ms PN sequence @ 110m

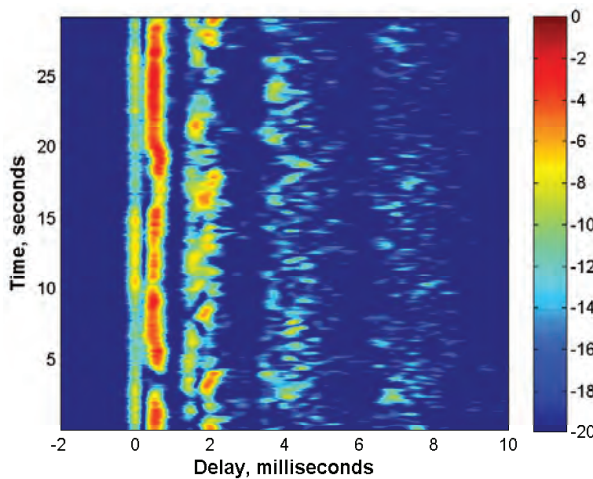


Figure 10. Normalised txrx correlation history (dB)–21ms PN sequence @ 500m

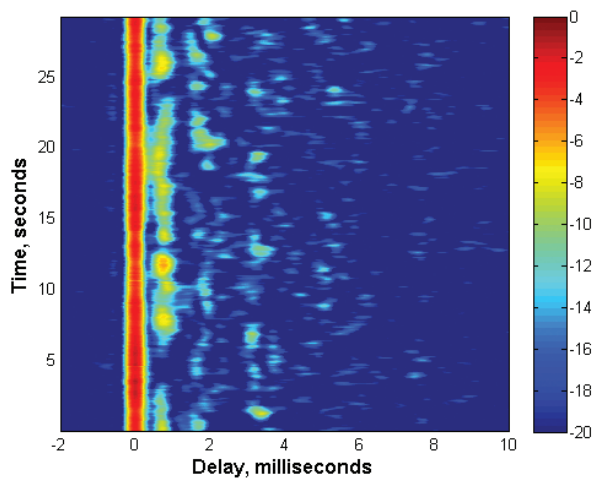


Figure 11. Normalised txrx correlation history (dB)–21ms PN sequence @ 1007m

EXPERIMENTAL DOPPLER SHIFT RESULTS

Spreading Function Doppler Shift Indication

The Spreading Functions corresponding to the 110m, 500m and 1007m ranges are presented in Figs. 12-14. The Spreading Functions are over-plotted with white markers representing the 3σ Doppler estimates from geometrical consideration as per Fig. 8, making use of the correspondence between Doppler frequency shift and velocity shift in Eq. (2). The corresponding delays of the white markers relate to an idealised waveguide with parallel boundaries. In reality the delays will vary with the path elongation and contraction associated with vertical surface movement, and with the moving reflection position linked to travelling surface waves. The variation in actual delay of surface-interacting paths is indicated by the substantial delay-spreading (x-axis) evident in the Spreading Function compared to the idealised discrete delay points.

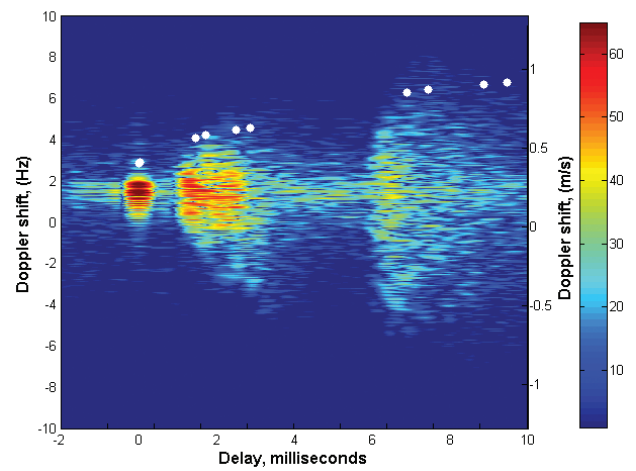


Figure 12. Spreading Function (dB) with 3σ geometrical Doppler estimates @ 110m

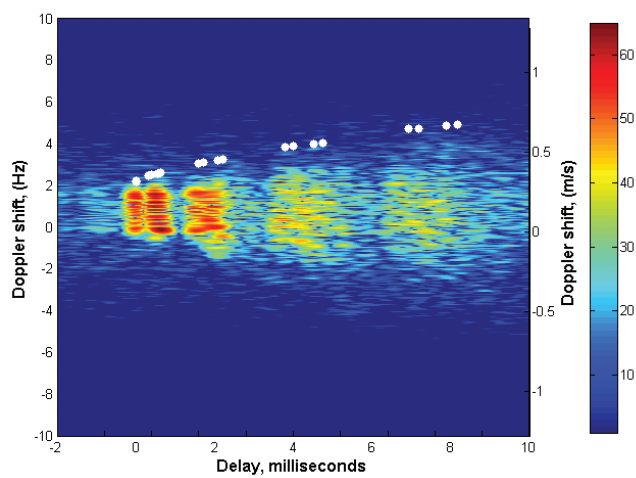


Figure 13. Spreading Function (dB) with 3σ geometrical Doppler estimates @ 500m

The 3σ estimates of total Doppler velocity shift from relative movement on idealised transmission paths and a simplistic treatment of surface wave movement readily account for Doppler shifted arrivals within 25dB-30dB of the strongest arrival at all delays. This Doppler estimate from velocity shift is therefore considered useful to interpretation of the Spreading Function Doppler.

Time domain Doppler search method

The results presented below relate to approximately the same channel as the 110m results in Fig. 9 and Fig. 12, but with transmitter drift extending the average range to 122m, and reducing the averaging closing speed from 0.19m/s to 0.13m/s.

Comparison of the short PN-sequence channel response history in Fig. 9 with the long PN-sequence channel response history in Fig. 15 illustrates how time varying channel Doppler degrades the txrx correlation for a relatively long 1.4s Doppler-sensitive sequence.

The correlation versus Doppler and time results presented in Figs. 16, 17 and 18 have been generated by block-by-block Doppler search for delay ranges relating to the first, second and third delayed path groups illustrated in Fig. 15. Whilst not shown, the equivalent Doppler frequency range of these figures is ± 10 Hz, as for the short-sequence spreading function plots.

The ‘ripples’ either side of the correlation maximum in Fig. 16 result from the ambiguity function Doppler side-lobes of the 1.4s PN sequence. The cyclical influence of swell orbital motion on relative motion is apparent in the Doppler time history for the first, second and third delay arrival groups. This time-dependent Doppler information is not obtainable from the Spreading Function or the time-domain channel response for the short 21ms sequence, for which the Doppler resolution of 6.1m/s is too coarse to enable detection of Doppler shift from orbital motion.

It appears from the time-domain Doppler analysis that there are no strong signal arrivals at large Doppler shift, however this

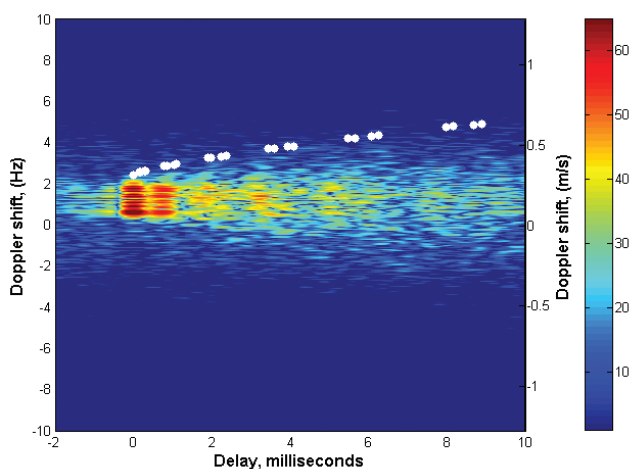


Figure 14. Spreading Function (dB) with 3σ geometrical Doppler estimates @ 1007m

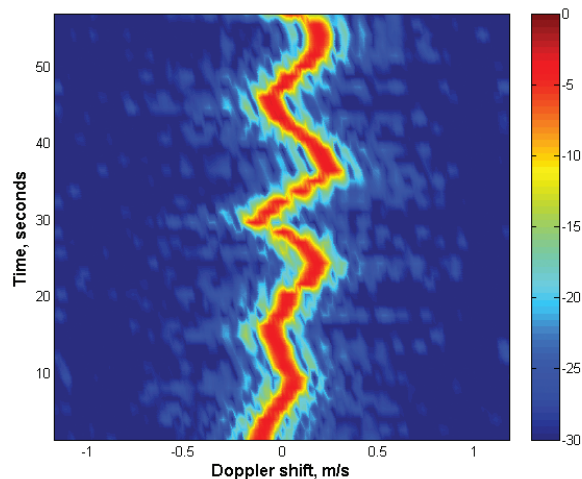


Figure 16. First arrivals normalised correlation (dB) versus time and Doppler, 1.4s PN sequence @ 122m

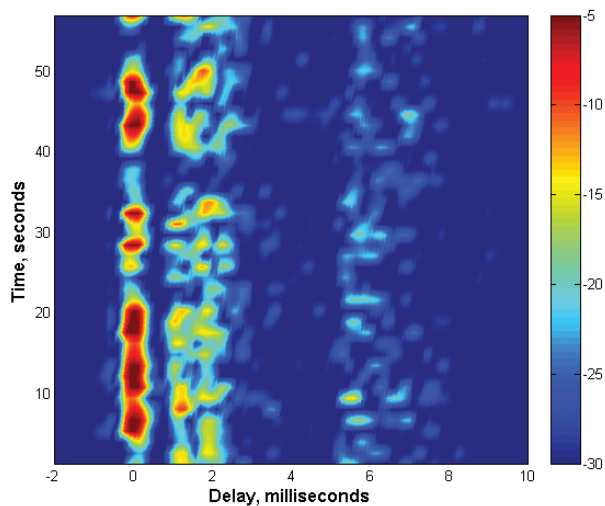


Figure 15. Normalised txrx correlation (dB)–1.4s PN sequence @ 122m

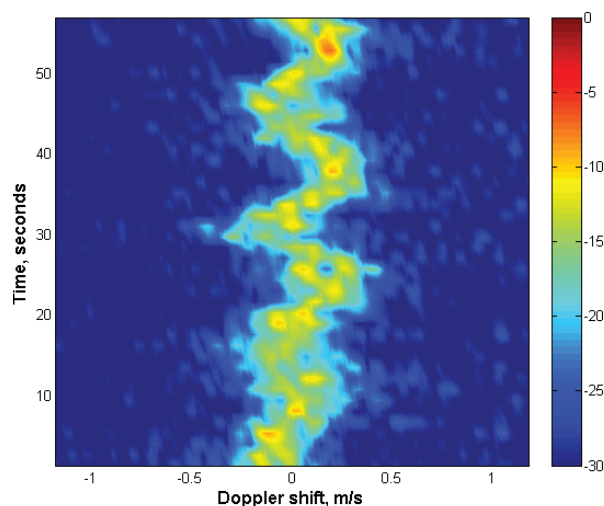


Figure 17. Second arrivals normalised correlation (dB) versus time and Doppler, 1.4s PN sequence @ 122m

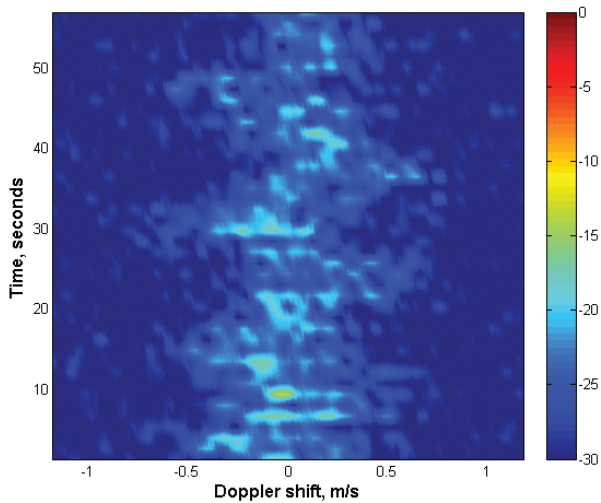


Figure 18. Third arrivals normalised correlation (dB) versus time and Doppler, 1.4s PN sequence @ 122m

does not exclude the possibility of such transients occurring at a significantly shorter time-scale than the 1.4s probe sequence. However the same time-domain analysis was conducted for the shorter 170ms PN-sequence channel response (0.75m/s Doppler resolution) (not presented), which also indicated the absence of isolated strong transients at high Doppler shift.

It is concluded that whilst the Doppler resolution by direct Doppler search is low, the time history provides valuable insights into channel behaviour from a channel modelling perspective.

CHANNEL COHERENCE

The coherence of the channel response was explored for the repeated 21ms probe sequence to investigate the channel response update rate that would be necessary for a high-fidelity channel simulator. Results corresponding to the 110m, 500m and 1007m channels are presented in Figs. 19, 20 and 21, respectively. Markers on the figures indicate the calculated coherence at 21ms intervals. The results for each channel represent the average of ten three-second sub-blocks of the full 30s sample. The coherence $C(t)$ of each sub-block is calculated for the response within a given delay range (τ_1, τ_2) relative to reference time t_0 by Eq. (10).

$$C(t) = \frac{\sum_{\tau_2}^{\tau_1} h^*(\tau, t_0)h(\tau, t)}{\sqrt{\sum_{\tau_2}^{\tau_1} h^*(\tau, t_0)h(\tau, t_0) \sum_{\tau_2}^{\tau_1} h^*(\tau, t)h(\tau, t)}} \quad (10)$$

The results in Figs. 19 to 21 demonstrate high coherence for the first arrival group at all ranges. Although the strength of subsequent correlation maxima generally degrades with range, the coherence of later arrivals generally improves with range, consistent with the geometrical trend of diminished in-path Doppler contributions from the moving sea surface as range increases.

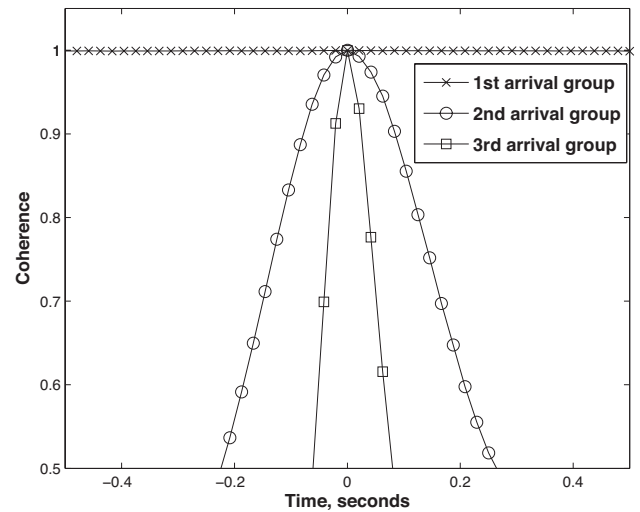


Figure 19. Channel coherence versus time and delay group @ 110m

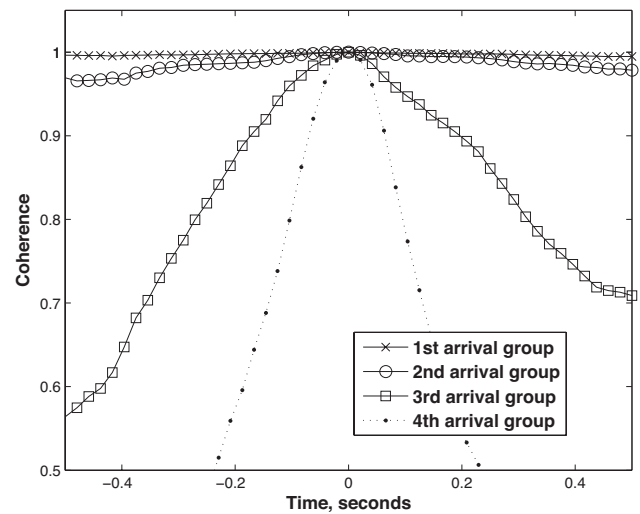


Figure 20. Channel coherence versus time and delay group @ 500m

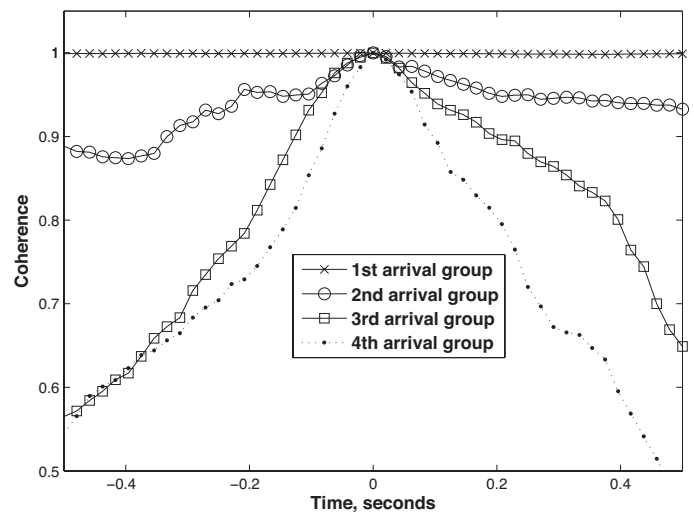


Figure 21. Channel coherence versus time and delay group @ 1007m

SUMMARY

Time and frequency domain analyses of experimental Doppler shift and delay spreading of underwater acoustic transmissions have been conducted for a shallow marine environment influenced by transmitter drift and heave, surface waves, and swell orbital motion. This analysis was conducted to ascertain channel coherence times and the significant sources and scale of channel Doppler spreading and delay spreading that need to be incorporated into a dynamic channel simulation for underwater communications.

The analysis has shown that the 3σ estimation of maximum channel Doppler shift in the units of equivalent velocity from simplified consideration of surface movement and relative motion is a useful approach to explaining the trends in experimental Doppler indicated by the Spreading Function.

Whilst the Doppler resolution achieved by direct Doppler search in the time domain is relatively low compared to that achievable by frequency domain analysis of a series of probe responses, it is concluded that the coarse Doppler time history provided by this approach is complementary to the Spreading Function in that it clarifies the origins of Doppler shifts associated with strong channel responses.

Coherence analysis of the channel response indicates that the coherence of later arrivals improves with increased transmission range, consistent with the geometrical trend of diminished in-path Doppler contributions from the moving sea surface as range increases.

ACKNOWLEDGMENTS

This project is supported under the Australian Research Council's Discovery Projects funding scheme (project number DP110100736) and by L3-Communications Oceania Ltd.

The authors would like to thank Frank Thomas and Malcolm Perry of the Centre for Marine Science and Technology (CMST) for technical support, and Dr Tim Gourlay of CMST for vessel motion instrumentation and data.

REFERENCES

- [1] S. Nordholm, Y. Rong, D. Huang, A. Duncan, "Increasing the range and rate of underwater acoustic communication systems using multi hop relay", Australian Research Council Discovery Project DP110100736, Curtin University, 2010.
- [2] T.H. Eggen, A.B. Baggeroer and J.C. Preisig, "Communication over Doppler spread channels – Part 1: Channel and receiver presentation", *IEEE Journal of Oceanic Engineering* **25**, 62-71 (2000)
- [3] P.A. van Walree, T. Jenserud and M. Smedsrud, "A discrete-time channel simulator driven by measured scattering functions", *IEEE Journal on Selected Areas in Communications* **26**, 1628-1637 (2008)
- [4] P.H. Dahl, "High frequency forward scattering from the sea surface: The characteristic scales of time and angle spreading", *IEEE Journal of Oceanic Engineering* **26**, 141-151 (2001)
- [5] P.A. van Walree, T. Jenserud and R. Otne, "Stretched-exponential Doppler spectra in underwater acoustic communication channels", *Journal of the Acoustical Society of America Express Letters* **128**(5), EL329-EL334 (2010)

Distance Learning for Acoustics

The Professional Education in Acoustics program was established some years ago on the request from the industry due to a lack of regularly available appropriate courses in the formal University programs. It is aimed at providing appropriate modules to meet the needs of those embarking on a career in Acoustics and has the support of the Association of Australian Acoustical Consultants (AAAC). It is also of value for those working in government agencies and allied organisations needing a fundamental understanding of acoustics. The program is based on a similar program that has been offered via universities and the UK Institute of Acoustics (IOA).

The program is fully flexible and all undertaken in distance learning mode. This means the modules can be commenced at any time and there is no requirement to complete at a specific date. This is an advantage to those who are unsure of future work demands – but of course a disadvantage as the lack of a deadline means that completion depends on the commitment of the registrant.

Each module of the program will be offered separately in distance learning mode so that it can be undertaken throughout Australia or elsewhere in the world and can be commenced at any time. Each module comprises course notes, assignments and two modules include practical exercises and a test. Registrants work through this material at their own pace and in their own location submitting the work electronically. The practical work and the test are undertaken at the registrant's location under supervision of their employer. It is expected that those registrants working for acoustical consultancies will receive support and supervision by their supervisors. For registrants who are working on the program without support from their employer will be given assistance by phone or email from the course coordinator. This assistance can be supplemented with assistance from a company that is a member of the AAAC.

For more information on the program see <http://www.aaac.org.au/au/aaac/education.aspx>